Open Archive Toulouse Archive Ouverte (OATAO)

OATAO is an open access repository that collects the work of Toulouse researchers and makes it freely available over the web where possible.

Stress intensity factors computation for bending plates with extended finite element method

Jérémie Lasry[1], Yves Renard[2] and Michel Salaün[3],[*],[†]

[1] *SAMTECH France, Centre AEROPARC, ZAC St-Martin du Touch 12, rue Caulet - Bat. A 14, F-31300 Toulouse, France*
[2] *Université de Lyon, CNRS, INSA-Lyon, ICJ UMR5208, LaMCoS UMR5259, F-69621, Villeurbanne, France*
[3] *Université de Toulouse; INSA, UPS, EMAC, ISAE; ICA (Institut Clément Ader), 10 av. E. Belin, F-31055 Toulouse, France*

SUMMARY

The modelization of bending plates with through-the-thickness cracks is investigated. We consider the Kirchhoff–Love plate model, which is valid for very thin plates. Reduced Hsieh–Clough–Tocher triangles and reduced Fraejis de Veubeke–Sanders quadrilaterals are used for the numerical discretization. We apply the eXtended Finite Element Method strategy: enrichment of the finite element space with the asymptotic bending singularities and with the discontinuity across the crack. The main point, addressed in this paper, is the numerical computation of stress intensity factors. For this, two strategies, direct estimate and J-integral, are described and tested. Some practical rules, dealing with the choice of some numerical parameters, are underlined.

1. INTRODUCTION

In the framework of linear elastic fracture mechanics, the computation of stress intensity factors (SIF) is one of the most important problems. Although some analytical solutions can be found in literature, they always correspond to simple geometries and loads. For general geometry and loading conditions, numerical methods have to be employed. So the goal of this paper is to investigate efficient numerical tools for very thin cracked plates, such as those that are widely used, for instance, in aircraft structures. Let us also remark that only through-the-thickness cracks will be considered here and that the material the plate is made of is homogeneous and isotropic.

So the first tool we use is eXtended Finite Element Method (XFEM). This is a strategy initially developed for plane elasticity cracked problems [1, 2], and it is now the subject of a wide literature (among many others, see [3–9] and references therein). It mainly consists in the introduction of the discontinuity across the crack and of the asymptotic displacements into the finite element space.

At the moment, there are few previous works devoted to the adaptation of XFEM to plate or shell models. In [10–12], shell models are used: because the near-tip asymptotic displacement in this model is unknown, no near-tip enrichment is used but only the discontinuous one. In particular, in [12, 13], the crack tip is always on an element edge: it means the crack spans entire elements of the mesh. Moreover, the Mindlin–Reissner theory is used, and the crack propagation is investigated, which is not the case of our work. In [14], which deals with cracked shells, the cracked part of the

---

domain is modelized by a three-dimensional XFEM formulation. It is matched with the rest of the domain and formulated with a classical finite element shell model. In this paper, a plate model is kept on the entire domain, and we consider singular enrichment. In [15], the plate model used is the Mindlin–Reissner one. However, in this reference, an important locking effect for thin plates has been detected despite the use of some classical locking-free elements. This suggests that this locking effect is due to the XFEM enrichment.

Even though most of the finite element codes are based on the Mindlin–Reissner plate model, the so-called Kirchhoff–Love model provides also a realistic description of the displacement for a thin plate because it is the limit model of the three-dimensional elasticity model when the thickness vanishes [16]. For instance, the panels used in aeronautic structures can be about a few millimeters thin, for several meters long. On this kind of plates, the shear effect can generally be neglected; consequently, the Kirchhoff–Love model is mechanically appropriate. It has already been used for the purpose of fracture mechanics (for instance, see [17]). Moreover, for through-thickness cracks, the limit of the energy release rate of the three-dimensional model can be expressed with the Kirchhoff–Love model solution [18, 19].

Because the Kirchhoff–Love model corresponds to a fourth-order partial differential equation, a conformal finite element method (FEM) needs the use of $\mathcal{C}^1$ (continuously differentiable) elements. We consider the reduced Hsieh–Clough–Tocher (HCT) triangle and the reduced Fraejis de Veubeke–Sanders (FVS) quadrilateral because they are the less costly conformal $\mathcal{C}^1$ elements [20]. In the XFEM framework, the knowledge of the asymptotic crack tip displacement is required. It is the case for a Kirchhoff–Love isotropic plate as it corresponds to the bi-Laplacian singularities [21]. Thanks to all this material, it was possible to derive an efficient XFEM for thin cracked plates with Kirchhoff–Love theory. It is detailed in [22], and some of its features, used in this paper, are recalled in the following.

Then, it is possible to introduce the second tool that deals with SIF computation. For this, two different strategies are suggested. The first one consists in a direct estimate. It follows an idea introduced in [23], for two-dimensional elasticity problem. And we have adapted it to our bending plate problem and our XFEM formulation. Let us remark that this approach lies on the SIF definition as the limit, when the distance, say r, to the crack tip tends to 0, of some stress multiplied by $\sqrt{r}$, up to a mutiplicative coefficient. In classical FEM, the stress is numerically evaluated and strongly depends on the mesh refinement. In [12], for plates, an alternative approach that uses the knowledge of the asymptotic singular displacements and the numerical evaluation of the displacements through what is called a displacement extrapolation technique is suggested. It will be explained later that we can directly use the singular displacements we have introduced in the numerical formulation. The second is more classical and uses J-integral. This is the way chosen in [15] for Mindlin–Reissner plates. In our case, we had to derive this approach for Kirchhoff–Love model.

The paper is organized as follows. Section 2 describes the model problem. Section 3 is devoted to the extended finite element discretization of the Kirchhoff–Love model. In Section 4, two strategies for SIF computation are detailed. In Section 5, numerical results, which illustrate the capabilities of these methods and enable the derivation of some practical rules for the choice of some numerical parameters, are presented and discussed. Finally, Section 6 provides concluding remarks.

2. THE MODEL PROBLEM

2.1. Notations and variational formulation

Let us consider a thin plate, that is a plane structure for which one dimension, called the thickness, is very small compared with the others. For this kind of structures, starting from *a priori* hypotheses on the expression of the displacement fields, a two-dimensional problem is usually derived from the three-dimensional elasticity formulation by means of integration along the thickness. Then, the unknown variables are set down on the midplane of the plate, denoted here by ω.

This midplane ω is an open subset of $\mathbb{R}^2$. In the three-dimensional Cartesian referential, the plate (Figure 1) occupies space
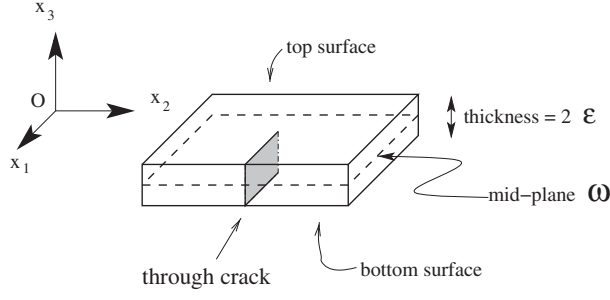
Figure 1. The cracked thin plate (the thickness is oversized for the sake of clarity).

$$\left\{ (x_1, x_2, x_3) \in \mathbb{R}^3 / (x_1, x_2) \in \omega \ \text{ and } x_3 \in]-\varepsilon; \varepsilon[\right\}.$$

So, the x_3 coordinate corresponds to the transverse direction, and all the midplane points have their third coordinate equal to 0. The thickness is 2ε. Finally, we assume that the plate has a through-the-thickness crack and that the material is homogeneous and isotropic and of Young's modulus E and Poisson's ratio ν.

In plate theory, the following approximation of the three-dimensional displacements is usually considered

$$\begin{cases} u_1(x_1, x_2, x_3) = \underline{u}_1(x_1, x_2) + x_3 \, \phi_1(x_1, x_2), \\ u_2(x_1, x_2, x_3) = \underline{u}_2(x_1, x_2) + x_3 \, \phi_2(x_1, x_2), \\ u_3(x_1, x_2, x_3) = u_3(x_1, x_2). \end{cases} \tag{1}$$

In these expressions, $\underline{u}_1$ and $\underline{u}_2$ are the membrane displacements of the midplane points, u_3 is the deflection, and ϕ_1 and ϕ_2 are the section rotations. In the case of an isotropic material, the variational formulation splits into two independent problems: the first, called the membrane problem, deals only with membrane displacements, whereas the second, called the bending problem, concerns deflection and rotations. The membrane problem corresponds to the classical plane elasticity problem and has been already treated in many references (see, for instance, [4,5]). So, here, we only consider the bending problem.

In industrial finite element codes, the most widely used plate model is the Mindlin–Reissner one, for which the displacement is given by (1). Nevertheless, for reasons mentioned in Section 1, we choose here to work with the Kirchhoff–Love model, which can be seen as a particular case of (1), as it is obtained by introducing the so-called Kirchhoff–Love assumptions, which read

$$\nabla u_3 + \phi = 0 \ \text{ i.e. } \ \begin{cases} \phi_1 = -\partial_1 \, u_3, \\ \phi_2 = -\partial_2 \, u_3, \end{cases} \tag{2}$$

where the notation ∂_α stands for the partial derivative with respect to x_α. A first consequence of this relation is that the transverse shear strain is identically zero, which avoids the shear locking problem. A second consequence of (2) is that the section rotation only depends on the transverse displacement. It means that this displacement is the only unknown function for the bending problem. For convenience, it will be denoted by u in the following. So, in the Kirchhoff–Love framework and for a pure bending problem, the three-dimensional displacement reads

$$\begin{cases} u_1(x_1, x_2, x_3) = -x_3 \, \partial_1 u(x_1, x_2), \\ u_2(x_1, x_2, x_3) = -x_3 \, \partial_2 u(x_1, x_2), \\ u_3(x_1, x_2, x_3) = u(x_1, x_2). \end{cases}$$

For the sake of simplicity, we assume the plate is clamped on its boundary and the crack faces are traction free. Then, the plate is subjected to a volume force, say f of coordinates (f_1, f_2, f_3),

and two surface forces, say g^+ and g^-, applied on the top and bottom surfaces. The variational formulation (or virtual work formulation) of the Kirchhoff–Love model reads as

$$\begin{cases} \text{Find } u \in H_0^2(\omega) \text{ such that for any } v \in H_0^2(\omega), \\ \displaystyle\int_\omega \frac{2E\varepsilon^3}{3(1-\nu^2)} \left[(1-\nu)\, \partial_{\alpha\beta}^2 u + \nu\, \Delta u\, \delta_{\alpha\beta} \right] \partial_{\alpha\beta}^2 v \; \mathrm{d}x = \int_\omega [Fv - M_\alpha\, \partial_\alpha v] \; \mathrm{d}x. \end{cases} \tag{3}$$

where

$$-F = \int_{-\varepsilon}^{\varepsilon} f_3 \; \mathrm{d}x_3 + g_3^+ + g_3^-, \text{ which is the resulting transverse loading,}$$

$$-M_\alpha = \int_{-\varepsilon}^{\varepsilon} x_3\, f_\alpha \; \mathrm{d}x_3 + \varepsilon(g_\alpha^+ - g_\alpha^-), \text{ which is the resulting moment loading.}$$

Moreover, $\delta_{\alpha\beta}$ stands for the Kronecker's symbol, and the summation convention over repeated indices is adopted, with Greek indices varying in $\{1, 2\}$. Finally, $H_0^2(\omega)$ is the classical Sobolev space of square integrable functions whose first and second derivatives in the distribution sense are square integrable and which vanish on the boundary, like their normal derivative (see [24], for instance).

2.2. Asymptotic displacement near the crack tip and fracture modes

In the Kirchhoff–Love plate model, there are two fracture modes. Applying a symmetric bending leads to the first fracture one, whereas applying an antisymmetric bending or a transverse shear leads to the second fracture mode (Figure 2).

To characterize them, let us recall that the governing equation related to the bending variational problem (3) reads

$$\frac{2E\varepsilon^3}{3(1-\nu^2)} \Delta^2 u = F + \partial_\alpha M_\alpha, \tag{4}$$

on the midplane ω. It is a bi-Laplacian problem for which the singularities are well known [21]. So, close to the crack tip, the displacement may be written as $u = u_r + u_s$, where u_r stands for the regular part of the transverse displacement and belongs to $H^3(\omega)$. The singular part u_s reads

$$u_s(r, \theta) = \mathcal{A}_{KL}\, r^{3/2} \left[K_1 \left(\frac{\nu+7}{3(\nu-1)} \, \cos\frac{3}{2}\theta + \cos\frac{\theta}{2} \right) + K_2 \left(\frac{3\nu+5}{3(\nu-1)} \, \sin\frac{3}{2}\theta + \sin\frac{\theta}{2} \right) \right] \tag{5}$$

in polar coordinates relatively to the crack tip (Figure 3), with

$$\mathcal{A}_{KL} = \frac{\sqrt{2}}{2} \frac{1-\nu^2}{E\varepsilon(3+\nu)}. \tag{6}$$

This singular displacement belongs to $H^{5/2-\eta}(\omega)$ for any $\eta > 0$. In addition, the scalar coefficients K_1 and K_2 are the so-called stress intensity factors, which are widely used in fracture mechanics for crack propagation.
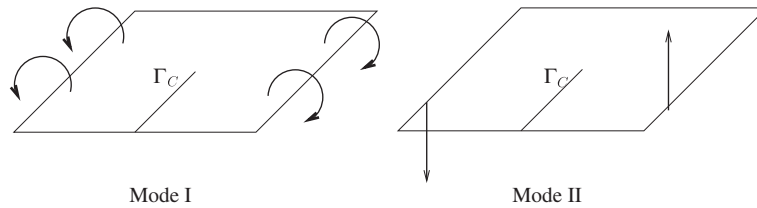

Figure 2. Fracture modes for Kirchhoff–Love bending model (Γ_C is the crack). Left: a symmetric bending leads to mode I. Right: a shear bending leads to mode II.
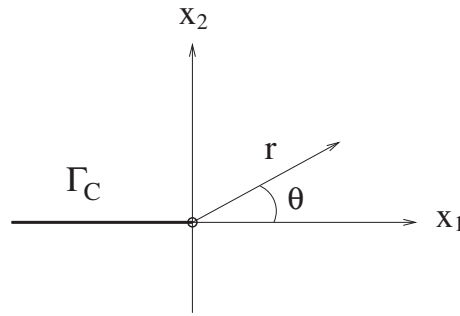
Figure 3. System of polar coordinates relative to the crack tip (the crack is in bold line).

To conclude, we recall that the Kirchhoff–Love plate theory corresponds to the limit of the three-dimensional elasticity theory when the thickness vanishes. However, the singularities we present here are deduced from the Kirchhoff–Love theory and not from the three-dimensional elasticity theory. The reader interested by the link between the singularities of these two theories is referred to [25].

3. EXTENDED FINITE ELEMENT APPROXIMATION OF THE KIRCHHOFF–LOVE MODEL

3.1. Classical finite element approximation

Let us introduce now the finite element discretization of the variational formulation (3). In order to have a conformal method, the finite element space V^h has to satisfy $V^h \subset H_0^2(\omega)$. This leads to the use of $\mathcal{C}^1$ finite elements. Among the available elements having this regularity, the reduced HCT triangles [20, p. 356–357] and FVS quadrangles [20, p. 359–360] are of particular interest. For both elements, the triangle (respectively quadrangle) is divided into three (respectively four) subtriangles (Figure 4). The basis functions are P_3 polynomials on each subtriangle and matched $\mathcal{C}^1$ across each internal edge. In addition, to decrease the number of degrees of freedom (dof), the normal derivative is assumed to vary linearly along the external edges of the elements (this assumption does not hold on the internal edges). At the end, there are only three dof on each node for both elements: the value of the function and its first derivatives. So, these elements have the two following advantages:

- The computational cost is limited to three dof for each node of the mesh, like a classical Mindlin–Reissner element (the deflection and the two section rotations).
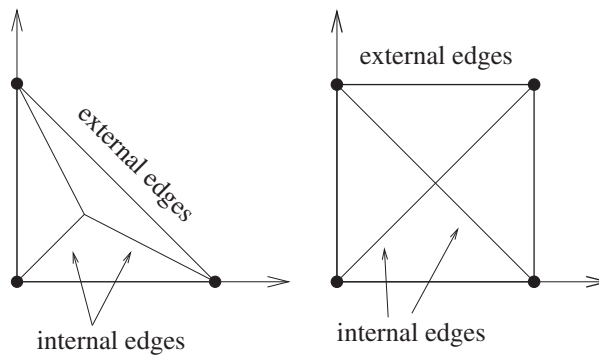

Figure 4. Hsieh–Clough–Tocher triangle and Fraejis de Veubeke–Sanders quadrangle. Location of degrees of freedom and subtriangles.

- The theoretical error is in $O(h)$ and $O(h^2)$ for the H^2 and L^2 norm (respectively), on regular problems (h stands for the mesh parameter). The minimum regularity assumption for this error estimate to hold is that the exact solution belongs to $H^3(\omega)$ [26].

So, the reduced HCT or FVS elements and standard Mindlin elements have the same features as far as numerical cost and accuracy are concerned.

3.2. Extended finite element method enrichment

To define our XFEM enrichment strategy, we follow ideas presented in previous papers [4, 5]. As usual, the discontinuity of the displacement across the crack is represented using Heaviside-like function, which is multiplied by the finite element shape functions. For the nonsmooth enrichment close to the crack tip, an enrichment area of fixed size is defined, and the nonsmooth functions are added inside all this area. The strategy that is used in this paper is inspired by the so-called XFEM dof gathering with pointwise matching, introduced in [4] and developed for plates in [22].

As noticed in [9], such function enrichment scheme does not satisfy a local partition of unity because enriched basis functions do not vanish at the edges of enriched elements. To solve this problem, the authors introduced the so-called shifted Heaviside function, which is of particular interest when the so-called branch functions, which reads $\sqrt{r}\cos(\theta/2)$ in their case, is not used for the enrichment, as they did in their paper. However, here, we use the branch functions. So we do not use the 'shifted' Heaviside function because, first, optimal convergence results for our finite element scheme were already obtained numerically [22] and, second, Nicaise *et al.* [27] have theoretically proven that an approach such as [4] is optimal.

Let us now describe more precisely the enrichment. So, let Γ be the boundary of the enrichment area (Figure 5). It cuts ω into two subdomains: the enrichment area, say ω_1, and the rest of the domain, say ω_2. Then, the support of the added singular functions is the whole enrichment area, but they are not multiplied by the finite element basis functions. So, instead of six additional dof per node inside the enrichment area, there are only two singular dof for the whole system. Consequently, if the unknowns defined on each subdomain ω_i are denoted by u_i^h, their expressions read

$$\begin{cases} u_1^h = \sum_{i \in N_1} a_i \, \varphi_i + \sum_{i \in J_1} b_i \, H \, \varphi_i + \sum_{i=1}^{2} c_i \, F_i, \\ u_2^h = \sum_{i \in N_2} a_i \, \varphi_i + \sum_{i \in J_2} b_i \, H \, \varphi_i, \end{cases} \tag{7}$$

where φ_i are the basis functions of the reduced HCT/FVS elements. The jump of H function is located on the crack; the set J denotes the dof whose shape function support is completely crossed by the crack (Figure 6). Furthermore, N_1 and N_2 are the sets of dof that are located in ω_1 and ω_2 ($N_1 \cap N_2$ is not empty and corresponds to the set of nodes that is on the boundary Γ). In the same
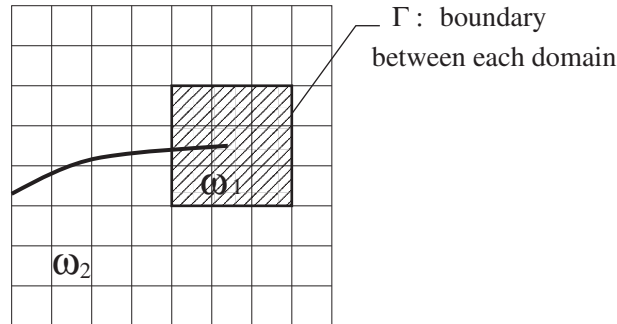

Figure 5. Set of elements that represents the support of the nonsmooth functions.
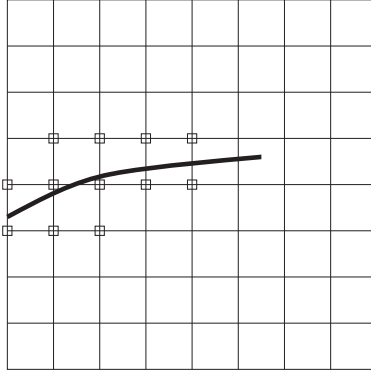
Figure 6. Set of nodes to be enriched along the crack.

way, J_i is the set of dof of J that is located in ω_i, and $J_1 \cap J_2$ is not empty for the same reason. Finally, the singular enrichment functions, derived from (5), are

$$
\begin{cases}
F_1 = r^{3/2} \left(\dfrac{\nu + 7}{3(\nu - 1)} \cos \dfrac{3}{2}\theta + \cos \dfrac{\theta}{2} \right), \\[3mm]
F_2 = r^{3/2} \left(\dfrac{3\nu + 5}{3(\nu - 1)} \sin \dfrac{3}{2}\theta + \sin \dfrac{\theta}{2} \right).
\end{cases}
$$

Naturally, a matching condition is needed at the interface between the enrichment area and the rest of the domain, in order to insure the continuity of the function and its derivatives. The following relations were chosen at this aim:

$$
\begin{cases}
\displaystyle \int_\Gamma u_1^h \, \lambda = \int_\Gamma u_2^h \, \lambda \,, & \forall \lambda \in \Lambda, \\[3mm]
\displaystyle \int_\Gamma \partial_n u_1^h \, \mu = \int_\Gamma -\partial_n u_2^h \, \mu \,, & \forall \mu \in M,
\end{cases}
$$

where Λ and M are appropriate multiplier spaces. Here, Λ is the space of piecewise polynomials of degree 2, and M is the space of the piecewise polynomials of degree 1, and we have checked in [22] that this choice keeps an optimal rate of convergence for the finite element scheme. Finally, let us observe the change of sign in front of the normal derivative $\partial_n u_i$ is because the outside normal vector has an opposite sign whether it is used in $\partial_n u_1^h$ or $\partial_n u_2^h$.

4. COMPUTATION OF STRESS INTENSITY FACTORS

In industrial applications dealing with cracked structures, the plate displacement is not straightforwardly meaningful in terms of crack propagation. The SIF are linked to the energy release rate G, and they provide such an information (we have $K_1^2 + K_2^2$ proportional to G). However, the calculation of SIF usually needs the use of some specific post-treatments, such as computation of J-integral.

4.1. First method: direct estimate

An interesting feature of the previously described methodology is that it can lead to a direct estimate of SIF. Comparing expressions of the asymptotic displacement (5) with that of the numerical displacement (7), it appears that, if the method is convergent, the finite element coefficients $(c_i)_i$ should be close to $(K_i)_i$, up to a multiplicative constant, which we shall calculate now.

Actually, in the expression of the singular displacement of Kirchhoff–Love theory (5), it appears as two singular modes. However, in the aforementioned XFEM formulation, the singular enrichments F_1 and F_2 are exactly these two singular functions. In particular, in the subdomain ω_1 containing the crack tip, the numerical solution reads

$$u_1^h = \sum_{i \in N_1} a_i \, \varphi_i + \sum_{i \in J_1} b_i \, H \, \varphi_i + \sum_{i=1}^{2} c_i \, F_i.$$

To show how coefficients c_i can be good approximations of SIF, up to a multiplicative constant to be determined, let us go back to the mathematical definitions of the SIF, in Kirchhoff–Love theory, which are

$$
\begin{aligned}
K_1 &= \lim_{r \to 0} \sqrt{2r} \, \sigma_{22}(r, \, \theta = 0, \, x_3 = \varepsilon), \\
K_2 &= \lim_{r \to 0} \frac{3 + \nu}{1 + \nu} \, \sqrt{2r} \, \sigma_{12}(r, \, \theta = 0, \, x_3 = \varepsilon).
\end{aligned}
\tag{8}
$$

The singular stresses are in $O(1/\sqrt{r})$ in the vicinity of the crack tip. However, if we calculate the components σ_{12} and σ_{22} resulting from numerical displacement u_1^h, multiply the result by $\sqrt{r}$, and make r tend to 0, all the regular terms are canceled and only the coefficients c_i remain, up to a multiplicative constant. So these coefficients fit well with the SIF definitions. We only have to evaluate the multiplicative constant.

Now, let us give the calculation in details for K_1, the same procedure being convenient for K_2. Under the assumption of isotropic and homogeneous material, we recall the link between σ_{22} and u:

$$\sigma_{22} = -x_3 \frac{E}{1 - \nu^2} \left[\nu \partial_{11}^2 u + \partial_{22}^2 u \right].$$

Replacing u by u_1^h in this expression and reporting it in (8) leads to

$$K_1^h = -\frac{E \, \varepsilon \sqrt{2}}{1 - \nu^2} \left(\nu \underbrace{\lim_{r \to 0} \sqrt{r} \, \partial_{11}^2 u_1^h}_{l_1} + \underbrace{\lim_{r \to 0} \sqrt{r} \, \partial_{22}^2 u_1^h}_{l_2} \right).$$

These two limits l_1 and l_2 exist. Because the most singular part of u_1^h is in $O(r^{3/2})$, we have $\partial_{\alpha\beta}^2 u = O(r^{-1/2})$. Apart from the crack, the element edges, and the internal boundaries of the HCT/FVS elements, the basis functions of u_1^h are C^2, so $\partial_{\alpha\beta}^2 u_1^h$ exists, and we have

$$\lim_{r \to 0} \sqrt{r} \, \partial_{\alpha\beta}^2 u_1^h = \lim_{r \to 0} \sum_i c_i \, \sqrt{r} \, \partial_{\alpha\beta}^2 F_i,$$

as

$$\lim_{r \to 0} \sqrt{r} \, \partial_{\alpha\beta}^2 \varphi_i = 0; \quad \lim_{r \to 0} \sqrt{r} \, \partial_{\alpha\beta}^2 \varphi_i \, H = 0.$$

The calculation of the second derivatives of F_i functions is not difficult and gives

$$
\begin{aligned}
\lim_{r \to 0} \sqrt{r} \, \partial_{11}^2 F_1(r, 0) &= \frac{\nu + 1}{\nu - 1}, \quad & \lim_{r \to 0} \sqrt{r} \, \partial_{22}^2 F_1(r, 0) &= \frac{\nu - 3}{\nu - 1}, \\
\lim_{r \to 0} \sqrt{r} \, \partial_{11}^2 F_2(r, 0) &= 0, \quad & \lim_{r \to 0} \sqrt{r} \, \partial_{22}^2 F_2(r, 0) &= 0.
\end{aligned}
$$

These expressions show that F_2 is not involved in the estimation of K_1^h. We deduce that $l_1 = c_1[(\nu + 1)/(\nu - 1)]$ and $l_2 = c_1[(\nu - 3)/(\nu - 1)]$, and finally,

$$K_1^h = -\frac{\sqrt{2} \, E \, \varepsilon \, (3 + \nu)}{1 \quad \nu^2} \, c_1.$$

The calculation for K_2 can be carried out the same way. The definition (8) involves σ_{12}, which is proportional to $\partial_{12}^2 u$. So, here, we have to calculate the cross derivatives of functions F_i and obtain

$$\lim_{r \to 0} \sqrt{r}\, \partial_{12}^2 F_1(r,0) = 0, \qquad \lim_{r \to 0} \sqrt{r}\, \partial_{12}^2 F_2(r,0) = \frac{\nu+1}{\nu-1},$$

which gives

$$K_2^h = -\frac{\sqrt{2}\, E\, \varepsilon\, (3+\nu)}{1-\nu^2}\, c_2.$$

As the numerical values of coefficients c_i result directly from the solving of the linear system associated with the calculation of u_1^h, no post-treatment is necessary to obtain approximations K_1^h and K_2^h of the SIF.

To conclude this section, let us remark that a similar idea has already been described and tested in [23]. In this paper, a numerical method, close to the one we propose here, is applied on a two-dimensional elasticity problem. This method uses the XFEM formulation named 'geometrical enrichment' in [5] and 'XFEM with fixed enrichment area' in [4], except that an enrichment zone of fixed area is not defined. The authors preferred to select from one to three layers of nodes surrounding the crack tip. Three meshes are used, the mesh parameter being divided by two at each refinement. With a single layer of enriched nodes, the error on the SIF is around 15%, and the mesh refinement does not improve significantly the accuracy. Adding a second layer of enriched nodes makes the error fall to globally 1% and, with the third layer, under 1%. However, this paper shows clearly that the mesh refinement does not lead to a strict decrease of the error. Finally, let us mention a recent work by Nicaise *et al.* [27] that shows a rather slow theoretical convergence of order $\sqrt{h}$ for bi-dimensional elasticity with XFEM.

4.2. Second method: J-integral computation

4.2.1. Method description and formulation. For Kirchhoff–Love theory, the expression of the J-integral has already been established in [17]. Its expression is

$$J = -\frac{1}{2} \int_\Gamma m_{\alpha\beta}\, \partial_{\alpha\beta} u\, b_1\, \mathrm{d}l \; + \; \int_\Gamma m_{\alpha\beta}\, b_\beta\, \partial_{1\alpha} u\, \mathrm{d}l - \int_\Gamma \partial_\alpha m_{\alpha\beta}\, b_\beta\, \partial_1 u\, \mathrm{d}l,$$

where $m_{\alpha\beta}$ stands for the bending moment and b_α for the outward unit vector normal to the contour of integration Γ. However, this expression is not the one used in numerical computations, because it does not allow separating the contributions of each SIF in the energy release rate. In addition, it needs to carry out integrations on contours, which is not well suited for finite element computations. The usual technique allowing to do accurate SIF calculations via J-integral is described in [1]. It is based upon works of Destuynder, described in details, for instance, in [19].

Now, the formulation adapted to the case of Kirchhoff–Love plate theory is presented. It follows quite closely the one described in [1], which deals with the case of two-dimensional elasticity. So, J-integral can be rewritten as

$$J = \int_\Gamma m_{\alpha\beta} \left(\partial_{1\alpha} u\, b_\beta - \frac{1}{2}\, \partial_{\alpha\beta} u\, b_1 \right)\, \mathrm{d}l - \int_\Gamma \partial_\alpha m_{\alpha\beta}\, b_\beta\, \partial_1 u\, \mathrm{d}l.$$

Following [1], we introduce two states. State (1) $\left(m_{\alpha\beta}^{(1)},\, u^{(1)} \right)$ matches the numerical solution of SIF that we want to evaluate. State (2) $\left(m_{\alpha\beta}^{(2)},\, u^{(2)} \right)$ is an auxiliary state corresponding to the asymptotic displacement of mode I or II, depending on the SIF we want to calculate. The J-integral for the sum of these two states reads

$$J^{(1+2)} = \int_\Gamma \left(m_{\alpha\beta}^{(1)} + m_{\alpha\beta}^{(2)} \right) \left[\left(\partial_{1\alpha} u^{(1)} + \partial_{1\alpha} u^{(2)} \right) b_\beta \; - \; \frac{1}{2} \left(\partial_{\alpha\beta} u^{(1)} + \partial_{\alpha\beta} u^{(2)} \right) b_1 \right]\, \mathrm{d}l$$

$$- \int_\Gamma \left(\partial_\alpha m_{\alpha\beta}^{(1)} + \partial_\alpha m_{\alpha\beta}^{(2)} \right) \left(\partial_1 u^{(1)} + \partial_1 u^{(2)} \right) b_\beta\, \mathrm{d}l.$$

It is developed as

$$J^{(1+2)} = J^{(1)} + J^{(2)} + I^{(1,2)}, \tag{9}$$

where $I^{(1,2)}$ is the so-called interaction integral:

$$I^{(1,2)} = \int_\Gamma \left(m_{\alpha\beta}^{(1)} \partial_{1\alpha} u^{(2)} + m_{\alpha\beta}^{(2)} \partial_{1\alpha} u^{(1)} \right) b_\beta - \frac{1}{2} \left(m_{\alpha\beta}^{(1)} \partial_{\alpha\beta} u^{(2)} + m_{\alpha\beta}^{(2)} \partial_{\alpha\beta} u^{(1)} \right) b_1 \, dl$$
$$- \int_\Gamma \left(\partial_\alpha m_{\alpha\beta}^{(1)} \partial_1 u^{(2)} + \partial_\alpha m_{\alpha\beta}^{(2)} \partial_1 u^{(1)} \right) b_\beta \, dl. \tag{10}$$

We introduce now the formula, established in [17], which links J-integral to SIF:

$$J = \frac{2\varepsilon\pi(1+\nu)}{3E(3+\nu)} \left(K_1^2 + K_2^2 \right).$$

We rewrite it in the case of the sum of the two states and find

$$J^{(1+2)} = J^{(1)} + J^{(2)} + 2\frac{2\varepsilon\pi(1+\nu)}{3E(3+\nu)} \left(K_1^{(1)} K_1^{(2)} + K_2^{(1)} K_2^{(2)} \right). \tag{11}$$

Because the right-hand sides of (9) and (11) are equal, we deduce

$$I^{(1,2)} = \frac{4\varepsilon\pi(1+\nu)}{3E(3+\nu)} \left(K_1^{(1)} K_1^{(2)} + K_2^{(1)} K_2^{(2)} \right).$$

So if, in this relation, state (2) is mode I (with $K_1^{(2)} = 1$ and $K_2^{(2)} = 0$), the value of the SIF K_1 is obtained with the value of the interaction integral, because the previous equation becomes

$$I^{(1,2)} = \frac{4\varepsilon\pi(1+\nu)}{3E(3+\nu)} K_1^{(1)}. \tag{12}$$

K_2 can be calculated in the same way.

4.2.2. Transformation of the interaction integral into a domain integral. The previous section shows that calculating interaction integral (10) with singular crack fields enables deducing the values of the SIF with (12). However, for numerical purpose, the interaction integral is transformed into a domain integral. Here again, we follow [1].

First, let us rewrite the interaction integral (10) in a more compact form:

$$I^{(1,2)} = \int_\Gamma \left(\mathcal{A}_\beta \, b_\beta + \mathcal{B} \, b_1 \right) \, dl,$$

with

$$\mathcal{A}_\beta = \left(m_{\alpha\beta}^{(1)} \partial_{1\alpha} u^{(2)} + m_{\alpha\beta}^{(2)} \partial_{1\alpha} u^{(1)} \right) - \left(\partial_\alpha m_{\alpha\beta}^{(1)} \partial_1 u^{(2)} + \partial_\alpha m_{\alpha\beta}^{(2)} \partial_1 u^{(1)} \right),$$
$$\mathcal{B} = -\frac{1}{2} \left(m_{\alpha\beta}^{(1)} \partial_{\alpha\beta} u^{(2)} + m_{\alpha\beta}^{(2)} \partial_{\alpha\beta} u^{(1)} \right).$$

The value of $I^{(1,2)}$ remains unchanged if the integrand is multiplied by a regular function, say q, whose value is 1 on the area defined by Γ and 0 on another contour C_0 that encloses Γ. So, if we assume there is no surface force applied on disc A defined by contour C_0, $I^{(1,2)}$ also reads

$$I^{(1,2)} = \int_\Gamma \left(\mathcal{A}_\beta \, B_\beta + \mathcal{B} \, B_1 \right) \, q \, dl,$$

where C is defined by $C = \Gamma \cup C_+ \cup C_- \cup C_0$, whereas B denotes the outward normal to C (Figure 7). Then, using divergence theorem and taking the limit of contour Γ, when Γ tends to the
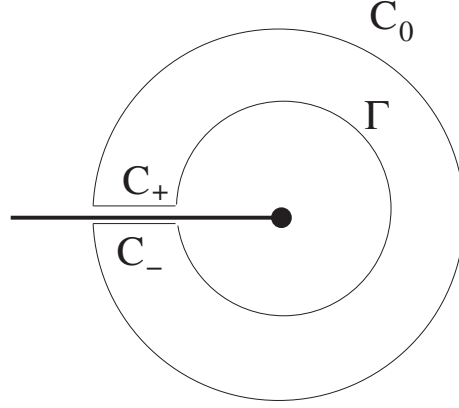
Figure 7. Integration contours for $I^{(1,2)}$ calculation.

point $(0, 0)$, the contour integral becomes a surface one, and domain A becomes the complete disc that contains the crack tip and that is bounded by C_0. Thus, we have

$$
\begin{aligned}
I^{(1,2)} &= \int_A \left[\partial_\beta \left(\mathcal{A}_\beta \, q \right) + \partial_1 \left(\mathcal{B} \, q \right) \right] \, \mathrm{d}A \\
&= \int_A \left[\left(\partial_\beta \mathcal{A}_\beta + \partial_1 \mathcal{B} \right) q + \mathcal{A}_\beta \, \partial_\beta q + \mathcal{B} \partial_1 q \right] \, \mathrm{d}A
\end{aligned}
$$

A direct calculation shows easily that $\partial_\beta \mathcal{A}_\beta + \partial_1 \mathcal{B} = 0$. Hence, we obtain

$$
\begin{aligned}
I^{(1,2)} = \int_A &\left[\left(m_{\alpha\beta}^{(1)} \, \partial_{1\alpha} u^{(2)} + m_{\alpha\beta}^{(2)} \, \partial_{1\alpha} u^{(1)} \right) - \left(\partial_\alpha m_{\alpha\beta}^{(1)} \, \partial_1 u^{(2)} + \partial_\alpha m_{\alpha\beta}^{(2)} \, \partial_1 u^{(1)} \right) \right] \partial_\beta q \, \mathrm{d}A \\
&- \frac{1}{2} \int_A \left(m_{\alpha\beta}^{(1)} \, \partial_{\alpha\beta} u^{(2)} + m_{\alpha\beta}^{(2)} \, \partial_{\alpha\beta} u^{(1)} \right) \, \partial_1 q \, \mathrm{d}A.
\end{aligned}
$$

Finally, setting $D = 2E\varepsilon^3/3(1 - \nu^2)$, we can observe that

$$
\begin{aligned}
m_{\alpha\beta}^{(1)} \, \partial_{\alpha\beta} u^{(2)} &= -D \left[(1 - \nu)\partial_{\alpha\beta}^2 u^{(1)} + \nu \, \Delta u^{(1)} \, \delta_{\alpha\beta} \right] \partial_{\alpha\beta}^2 u^{(2)} \\
&= -D \left[(1 - \nu)\partial_{\alpha\beta}^2 u^{(1)} \, \partial_{\alpha\beta}^2 u^{(2)} + \nu \, \Delta u^{(1)} \, \Delta u^{(2)} \right] = m_{\alpha\beta}^{(2)} \, \partial_{\alpha\beta} u^{(1)}.
\end{aligned}
$$

Hence, the final expression of interaction integral reads

$$
\begin{aligned}
I^{(1,2)} = \int_A &\left[\left(m_{\alpha\beta}^{(1)} \, \partial_{1\alpha} u^{(2)} + m_{\alpha\beta}^{(2)} \, \partial_{1\alpha} u^{(1)} \right) - \left(\partial_\alpha m_{\alpha\beta}^{(1)} \, \partial_1 u^{(2)} + \partial_\alpha m_{\alpha\beta}^{(2)} \, \partial_1 u^{(1)} \right) \right] \partial_\beta q \, \mathrm{d}A \\
&- \int_A m_{\alpha\beta}^{(1)} \, \partial_{\alpha\beta} u^{(2)} \, \partial_1 q \, \mathrm{d}A.
\end{aligned}
\tag{13}
$$

4.2.3. Numerical calculation of the interaction integral. Now, our purpose is to calculate the interaction integral $I^{(1,2)}$ given by (13), in the case of Kirchhoff–Love model, treated with reduced HCT/FVS elements. Expression (13) contains three terms. There is no difficulty for the two ones that contain the bending moments $m_{\alpha\beta}^{(i)}$ without derivatives. But the third term, which includes $\partial_\alpha m_{\alpha\beta}^{(i)}$, is harder to handle, as it involves third-order derivatives of the displacements. On the one hand, the functions we integrate are surely not in $H^3(\Omega)$. On the other hand, it cannot be expected that the third derivatives of a function may be correctly approximated by reduced HCT/FVS elements: for these elements, error estimates are only obtained up to the second derivatives. So we will transform (13) in order to avoid these third derivatives.

The expression we want to modify reads

$$X = -\int_A \left(\partial_\alpha m_{\alpha\beta}^{(1)} \, \partial_1 u^{(2)} + \partial_\alpha m_{\alpha\beta}^{(2)} \, \partial_1 u^{(1)} \right) \partial_\beta q \, \mathrm{d}A.$$

It is split into two terms:

$$X = \underbrace{-\int_A \partial_\alpha m_{\alpha\beta}^{(1)} \, \partial_1 u^{(2)} \, \partial_\beta q \, \mathrm{d}A}_{X_1} \underbrace{-\int_A \partial_\alpha m_{\alpha\beta}^{(2)} \, \partial_1 u^{(1)} \, \partial_\beta q \, \mathrm{d}A}_{X_2}.$$

X_2 can be computed without any particular difficulty, as it depends only on the crack tip singular functions. It only needs computation of third derivatives of these singularities. X_1 is integrated by parts:

$$X_1 = \underbrace{\int_A m_{\alpha\beta}^{(1)} \, \partial_\alpha (\partial_1 u^{(2)} \, \partial_\beta q) \, \mathrm{d}A}_{X_{11}} - \underbrace{\int_{\partial A} m_{\alpha\beta}^{(1)} \, \partial_1 u^{(2)} \, \partial_\beta q \, b_\alpha \, \mathrm{d}l}_{X_{12}}.$$

There is no problem concerning X_{11}. As far as X_{12} is concerned, in the case where $u^{(2)}$ is the exact mode I, it can be checked that $\partial_1 u^{(2)}$ cancels along the crack (this term cancels when $\theta = \pi$) and then $X_{12} = 0$. But in the case of mode II, X_{12} calculation is more difficult: this term differs from 0 but only along the crack where $\partial_\beta q$ is not 0. It is along the intersection between the crack and the boundary of the ring of integration. Nevertheless, in our numerical tests, for mode II, we shall neglect this term. Despite this simplification, computations of K_2 were not less precise than those of K_1.

To conclude this section, let us present briefly some features of numerical implementation. The calculation of interaction integral $I^{(1,2)}$ needs to define explicitly function q. Let us recall that this function is identically equal to 1 inside an area containing the crack tip and 0 outside a zone enclosing the first one, and q matches regularly from one zone to the other. Because only derivatives of q are needed in (13), those functions differ from 0 on a ring between the two zones. In practice, we define a ring of elements around the crack tip on which the J-integral is evaluated (Figure 8). In our numerical tests, this ring is made of elements located at a certain distance $\mathcal{R}_J$ from the crack tip. Furthermore, the function q is represented on the reduced HCT/FVS basis. The nodal values are set to 1 on the internal boundary of the ring and to 0 on the external boundary, whereas the dof associated to the derivatives are set to 0 on both boundaries.
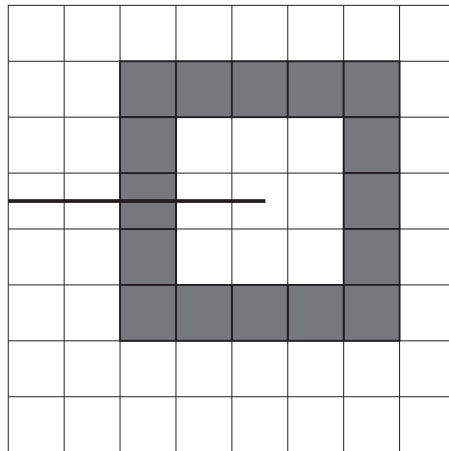

Figure 8. Ring of elements enclosing the crack tip.

5. NUMERICAL RESULTS

5.1. Description of the numerical study

The numerical experiments presented in this section were performed with the open-source finite element library Getfem++ [28].

5.1.1. Test cases. Two test cases with a straight-through crack are considered in this paper. The solution of the first one is the sum of the two singular modes:

$$u^{ex} = F_1 + F_2.$$

The sides of the crack follow a free edge condition. On the rest of the domain boundary, a nonhomogeneous Dirichlet condition, whose value corresponds to u^{ex}, is given. Consequently, the exact values of K_1 and K_2 are $1/\mathcal{A}_{KL}$, where $\mathcal{A}_{KL}$ is defined by (6). Finally, the plate we took is the square $[-0.5, 0.5] \times [-0.5, 0.5]$, with the crack tip at the origin.

The second test case is more classical and comes from [29]. It consists in a square plate with a central straight-through crack of length $2a$, and a constant moment M_0 is applied on the edges parallel to the crack (Figure 9). The dimensions of the plate are said to be 'infinite', which means that reference SIF values are correct only if the crack is small compared with the dimensions of the plate. These reference values are

$$K_1 = \frac{3\,M_0\,\sqrt{a}}{2\,\varepsilon^2}; \quad K_2 = 0.$$

For the numerical tests, we took a plate of edge 1, with a crack of size $2a = 0.22$. This remains significant compared with that in [30], where calculations are carried out with $2a = 0.18$. Because the problem is symmetric, only half of the domain is considered.

5.1.2. Goals of the study. The aim of the numerical experiments is to study the error made by our SIF calculation methods, with respect to the following parameters:

- mesh parameter h;
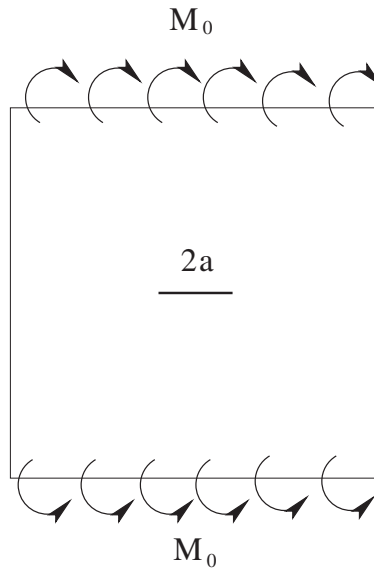- enrichment radius $\mathcal{R}$, which corresponds to the 'size' of ω_1 (Figure 5);

Figure 9. Second test case. Plate with central crack subjected to moments applied on two edges.

- integration ring radius $\mathcal{R}_J$, for J-integral method only; and
- structured or nonstructured meshes.

In addition, for J-integral, results are compared with that of nonenriched FEM.

Another goal of these numerical experiments is to bring elements of answer to the question of the influence of parameters $\mathcal{R}$ and $\mathcal{R}_J$ and to propose eventually some practical rules for the choice of these parameters, depending on the mesh size h. Indeed, in [5] and [4], the enrichment area is a disc, of radii 0.05 and 0.1, respectively. In [22], we took $\mathcal{R} = 0.15$. However, in a more general manner, we think the choice of $\mathcal{R}$ depends on the result we try to set. For example, to show the convergence of an enriched FEM in L^2 or H^2 norm, taking a fixed value independent of h is convenient. Nevertheless, on the most refined meshes, the choice of fixed $\mathcal{R}$ leads to enrich numerous layers of elements, which may be not necessary if we use only one mesh. So, in our study, we introduce two strategies for the choice of the size $\mathcal{R}$ of enriched domain ω_1. First, we consider several fixed values of $\mathcal{R}$. Second, $\mathcal{R}$ depends on h, in such a way that the enrichment area covers several layers of elements around the crack tip. It means $\mathcal{R}$ is equal to kh, where k is an integer we have taken between 1 and 5. Let us remark also that taking $\mathcal{R} = h$ is very close to the first XFEM formulation [1, 15], where only the element containing the crack tip is enriched by singular functions. Finally, as the results with the fixed value of $\mathcal{R}$ were not more accurate than those with $\mathcal{R}$ depending on h, we only present results with $\mathcal{R} = kh$ in this paper. For more details, the reader is referred to [31].

5.2. Direct estimate

This first method was tested on the two aforementioned test cases, with triangular and quadrangular, structured and nonstructured meshes, for several values of the mesh parameter h. Moreover, we have tested $\mathcal{R} = kh$, where k goes from 1 to 5.
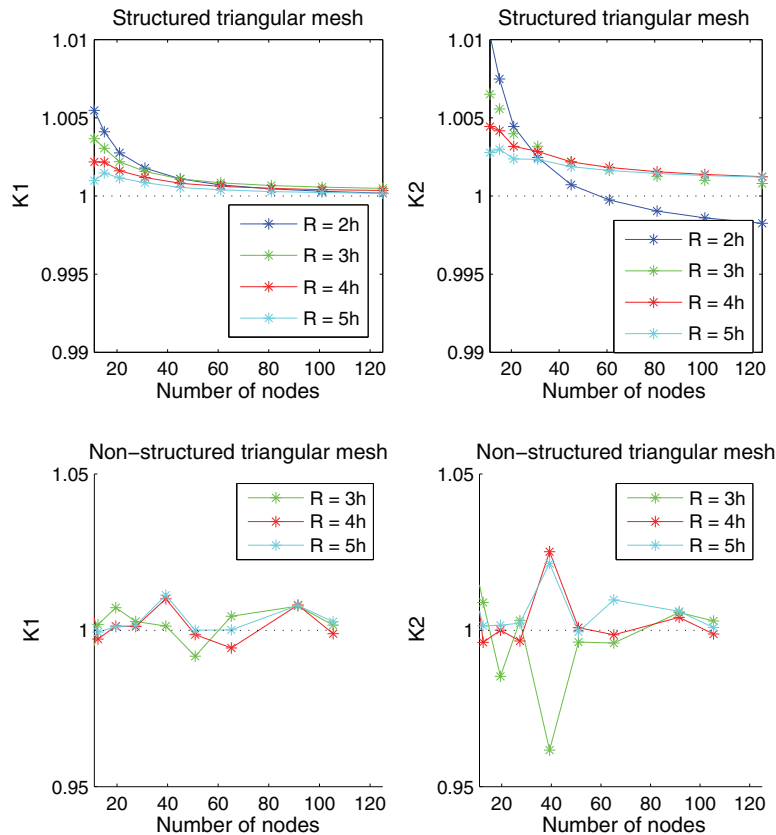

Figure 10. Stress intensity factors calculations—Direct estimate—First test case—Triangular meshes.

The results for the first test case are given in Figures 10 and 11. They show that the method provides very good estimates of SIF. The relative error is always lower than 5% and often lower than 1%. Let us remark that an error of 5% is precise enough for many industrial applications. Nevertheless, the convergence can be very slow on nonstructured meshes. Maybe it is due to high conditioning of the method, which reaches 10^{12} on such meshes.

For the second test case, the size of the crack is $a = 0.11$ on half domain, which is the rectangle $[0, 0.5] \times [-0.5, 0.5]$. So the crack is smaller than in the first test case. Moreover, the enrichment area must not touch the boundary $0 \times [-0.5, 0.5]$, because it corresponds to a symmetry condition. Indeed, singular enrichment does not satisfy this condition. Here, we use meshes, of which the level of refinement is equivalent to those of the first test case. It leads to a more drastic constraint on the choice of $\mathcal{R}$. We also tested the same values of k, but a high value of k needs a more important initial level of refinement. For example, for $k = 5$, the less refined mesh, in structured quadrangular meshes, needs around 60 elements on the longest edge of the domain. This explains why some curves are not complete. However, when this level of refinement is reached, the error is lower than 5%. The results are presented in Figure 12.

Despite its slow convergence, the 'direct estimate' method is simple and efficient and provides SIF values close to the exact ones. According to the tests, increasing $\mathcal{R}$ improves the results. So, because of the slow convergence, it may be more interesting to increase $\mathcal{R}$ than to refine the mesh. We observe also that $\mathcal{R} = 5h$ enables reaching always a satisfactory accuracy. It leads us to propose the following practical rule. Given a crack of length a, the domain has to be meshed with a minimum h around $a/5$, and the radius of the enrichment area is taken equal to $5h$. Let us remark that this rule indicates that the smaller the crack is, the more the mesh has to be refined in order to take care of the crack. This is in accordance with intuition: the smaller a crack is compared with element size, the less it has influence on global solution. A very refined mesh is then necessary in order to 'catch' its effect.
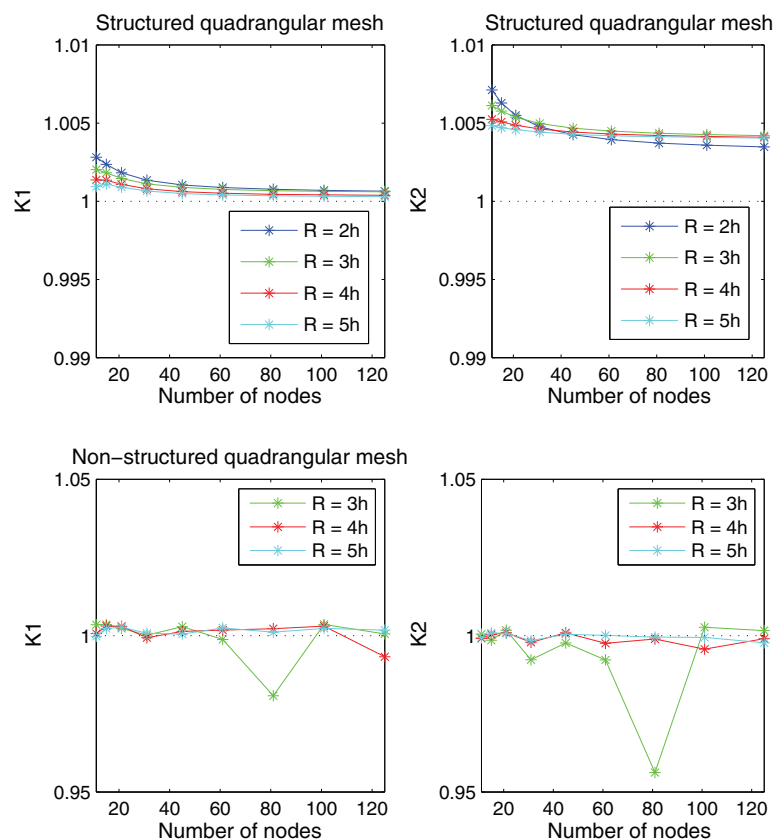

Figure 11. Stress intensity factors calculations—Direct estimate—First test case—Quadrangular meshes.
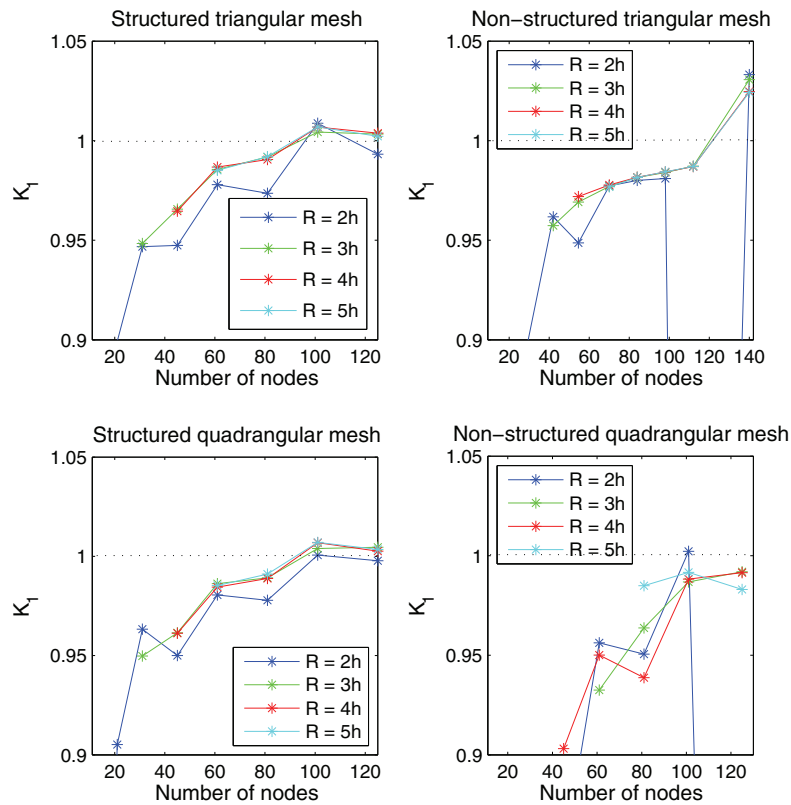
Figure 12. Stress intensity factors calculations—Direct estimate—Second test case.

5.3. J-integral

The same numerical experiments as with the previous section were carried out. But, here, the radius of the ring of integration $\mathcal{R}_J$ has also been investigated.

5.3.1. First test case. We have observed that, even if the results are accurate, from one mesh to another, the error is not strictly decreasing, as the value provided by J-integral oscillates around the exact value. Hence, a mesh can give an error slightly greater than a coarser one. That is why we give convergence curves only on the first test case and on structured meshes, for which less oscillatory results are obtained.
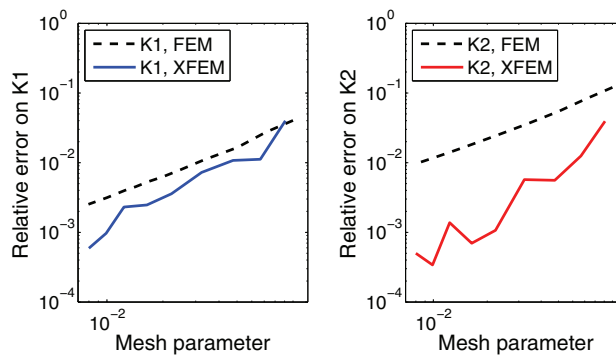

Figure 13. Stress intensity factors convergence curves—J-integral—First test case—Triangular meshes.

So Figures 13 and 14 present convergence curves for structured meshes, both triangular and quadrangular. For this particular purpose, the radius of the enrichment area $\mathcal{R}$ must be fixed, and it is equal to 0.15 here. The comparison with a nonenriched FEM shows that XFEM improves the SIF values and that the rate of convergence may be slightly better.
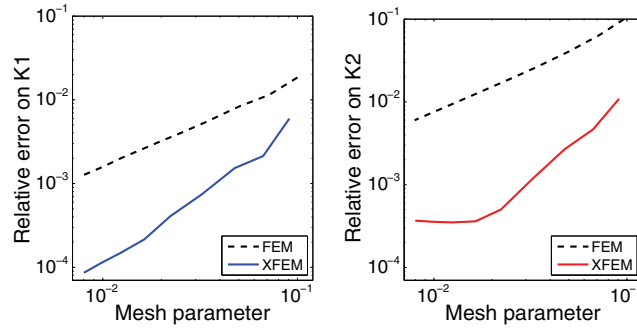

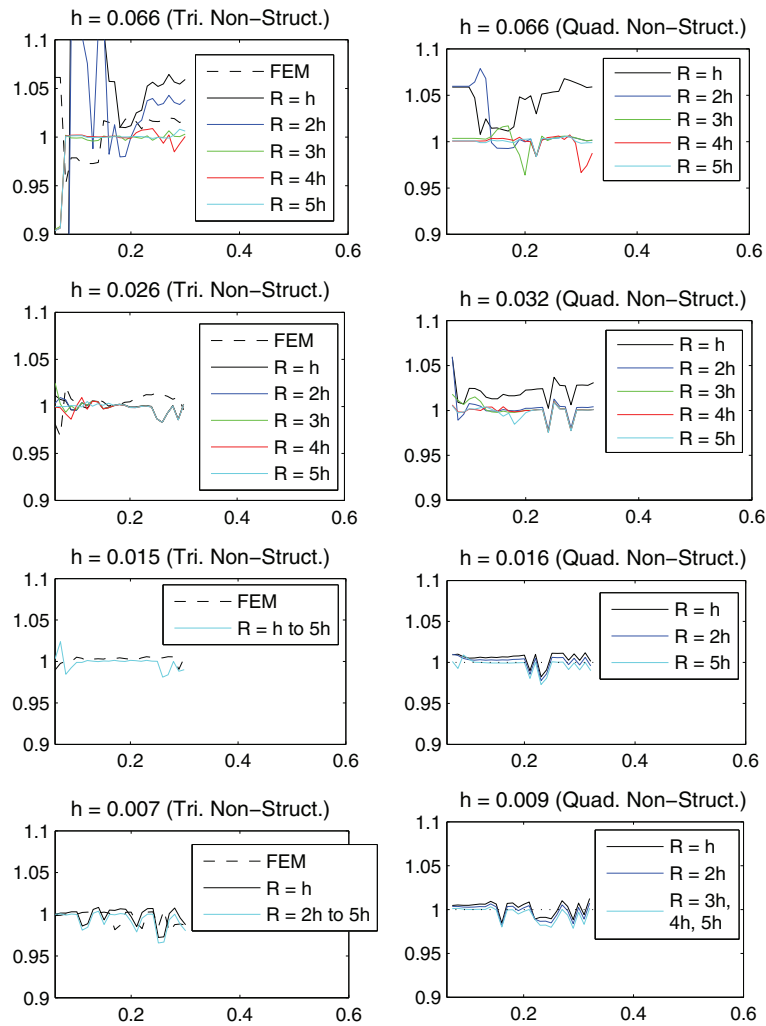Figure 14. Stress intensity factors convergence curves—J-integral—First test case—Quadrangular meshes.

Figure 15. Normalized K_1 versus $\mathcal{R}_J$—J-integral—First test case.

Now, let us present a more global study in which the numerical values of SIF are investigated, with respect to h, $\mathcal{R}$, and $\mathcal{R}_J$. Figure 15 gives results for $\mathcal{R} = kh$ on nonstructured triangular and quadrangular meshes. Moreover, only results on K_1 were shown, with curves for K_2 being very similar [31]. For brevity, we do not present structured meshes' results. In fact, they do not bring additional information, and they have already been presented in the case of direct estimate (Figures 13 and 14).

So, our results show that the error often remains lower than 5%. On structured meshes, this error is generally less than 1% [31]. On nonstructured meshes, taking $\mathcal{R} = 3h$ is enough to obtain an error lower than 5% on all meshes. Such a value for $\mathcal{R}$ seems to be minimal. Besides, on coarser meshes, with $\mathcal{R} = h$, the error is often greater than 10%.

All in all, results are relatively stable with respect to ring radius $\mathcal{R}_J$. To conclude, it can be observed that Figure 15 shows oscillations. Let us notice that it is not the case for regular meshes [31]. That is why we explain it by the fact that, in our calculations, the ring of integration is only a one-element width, which may be too irregular on nonstructured meshes to have stable results. Naturally, this explanation should be numerically tested. However, the error level on SIF appears to be good enough to avoid a more complex estimate.
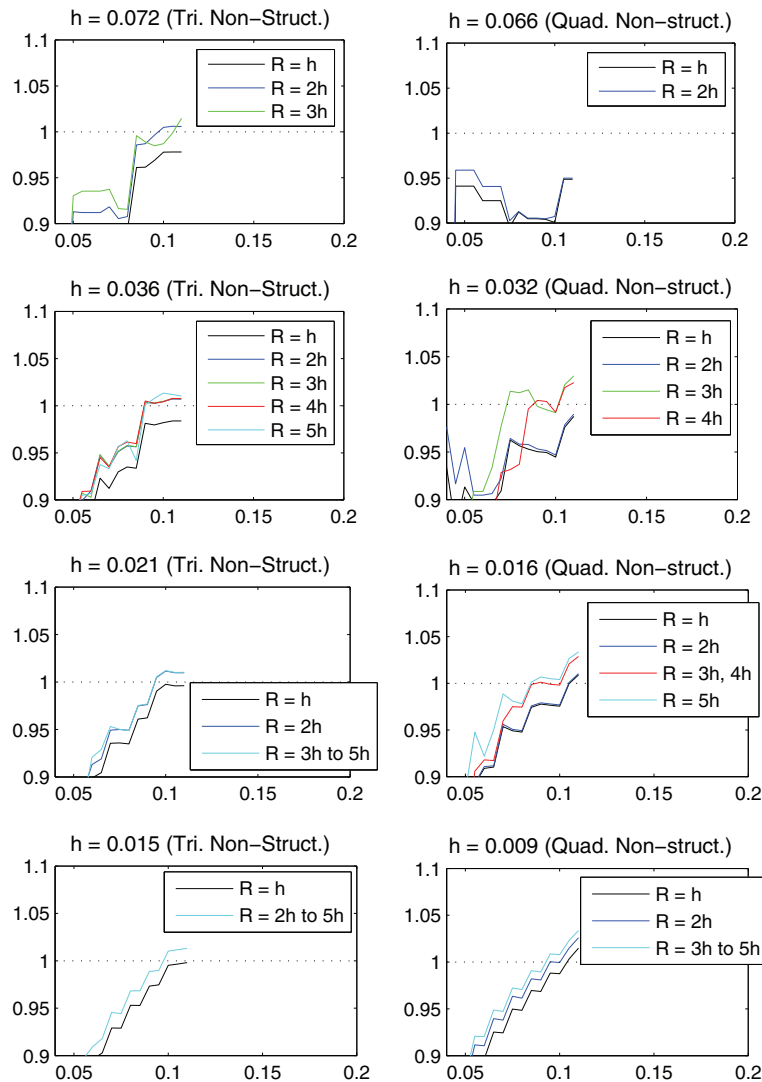

Figure 16. Normalized K_1 versus $\mathcal{R}_J$—J-integral—Second test case.

5.3.2. Second test case. We recall that the crack is smaller here, which limits the choice of $\mathcal{R}$ and $\mathcal{R}_J$. Again, we take $\mathcal{R} = 3h$ for $k = 1, \ldots, 5$. In all cases, the radius of the ring of integration $\mathcal{R}_J$ varies from 0.05 to 0.11, so that this ring can touch the boundary. Our results tend to show that the precision depends mainly on $\mathcal{R}_J$. When $\mathcal{R}_J$ increases, the approximate SIF is closer to the exact one, and the best values are obtained for the greatest. Finally, except with coarser meshes, the best value is always lower than 5%, whereas the meshes with less than two elements on the crack induces significant errors. Numerical results are brought together in Figure 16 for nonstructured meshes.

To conclude on this second test case, we observe that a ring of integration having a great value as possible must be chosen, in order to have the most accurate SIF. Then, the rule of construction, we propose, is still to take $h = a/5$ (for a crack of length a) and $\mathcal{R} = 5h$.

6. CONCLUDING REMARKS

This paper addresses the modelization of bending plates with through-the-thickness cracks in the framework of linear elastic fracture mechanics. As very thin plates are considered, the Kirchhoff–Love plate model is used. The main point, studied in this paper, is the numerical computation of SIF. For that purpose, two strategies are described and evaluated on two test cases.

First, the 'direct estimate' method is simple and efficient and provides SIF values close to the exact ones. According to the tests, increasing the radius $\mathcal{R}$ of the enrichment area improves the results. Moreover, it seems more interesting to increase $\mathcal{R}$ than to refine the mesh. Second, a 'J-integral' approach, which gives also good results, is derived. Furthermore, the comparison with a classical FEM shows that XFEM improves the SIF values.

Finally, a practical rule may be emphasized. In all our tests, a radius $\mathcal{R} = 5h$ enables reaching always a satisfactory accuracy, for both SIF computation strategies. To make it possible, it leads to the following mesh rule. Given a crack of length a, the domain has to be meshed with a minimum h around $a/5$, and the radius of the enrichment area will be taken equal to $5h$.

Naturally, some developments and applications of this work have to be done. The first one deals with crack propagation as in [7, 12, 13]. The second one, which is more challenging, concerns cohesive models and shells, for which ideas developed in [9, 12, 13], among others, are a good starting point.

REFERENCES

1. Moës N, Dolbow J, Belytschko T. A finite element method for crack growth without remeshing. *International Journal for Numerical Methods in Engineering* 1999; **46**:131–150.
2. Moës N, Belytschko T. XFEM : nouvelles frontières pour les éléments finis. *Revue européenne des éléments finis* 1999; **11**:131–150.
3. Moës N, Gravouil A, Belytschko T. Non-planar 3D crack growth by the extended finite element and level sets, part I: mechanical model. *International Journal for Numerical Methods in Engineering* 2002; **53**:2549–2568.
4. Laborde P, Pommier J, Renard Y, Salaün M. High order extended finite element method for cracked domains. *International Journal for Numerical Methods in Engineering* 2005; **64**:354–381.
5. Béchet E, Minnebo H, Moës N, Burgardt B. Improved implementation and robustness study of the X-FEM for stress analysis around cracks. *International Journal for Numerical Methods in Engineering* 2005; **64**:1033–1056.
6. Sukumar N, Huang ZY, Prévost J-H, Suo Z. Partition of unity enrichment for bimaterial interface cracks. *International Journal for Numerical Methods in Engineering* 2004; **59**:1075–1102.
7. Areias PMA, Belytschko T. Analysis of three-dimensional crack initiation and propagation using the extended finite element method. *International Journal for Numerical Methods in Engineering* 2005; **63**:760–788.
8. Bordas S, Moran B. Enriched finite elements and level sets for damage tolerance assessment of complex structures. *Engineering Fracture Mechanics* 2006; **73**:1176–1201.

9. Zi G, Belytschko T. New crack-tip elements for XFEM and applications to cohesive cracks. *International Journal for Numerical Methods in Engineering* 2003; **57**:2221–2240.

10. Areias PMA, Song JH, Belytschko T. Analysis of fracture in thin shells by overlapping paired elements. *Computer Methods in Applied Mechanics and Engineering* 2006; **195**:5343–5360.

11. Areias PMA, Belytschko T. Analysis of finite strain anisotropic elastoplastic fracture in thin plates and shells. *Journal of Aerospace Engineering* 2006; **19**:259–270.

12. Areias PMA, Belytschko T. Non-linear analysis of shells with arbitrary evolving cracks using XFEM. *International Journal for Numerical Methods in Engineering* 2005; **62**:384–415.

13. Song JH, Belytschko T. Dynamic fracture of shells subjected to impulsive loads. *ASME Journal of Applied Mechanics* 2009; **76**:051301.

14. Wyart E, Coulon D, Duflot M, Pardoen T, Remacle J-F, Lani F. A sustructured FE-shell/XFE-3D method for crack analysis in thin-walled structures. *International Journal for Numerical Methods in Engineering* 2007; **72**:757–779.

15. Dolbow J, Moës N, Belytschko T. Modeling fracture in Mindlin-Reissner plates with the extended finite element method. *International Journal of Solids and Structures* 2000; **37**:7161–7183.

16. Ciarlet PG, Destuynder Ph. A justification of two-dimensionnal linear plate model. *Journal de M'ecanique* 1979; **18**:315–344.

17. Hui CY, Zehnder AT. A theory for the fracture of thin plates subjected to bending and twisting moments. *International Journal of Fracture* 1993; **61**:211–229.

18. Destuynder Ph. *Une Théorie Asymptotique des Plaques Minces en Élasticité Linéaire*. Masson: Paris, 1986.

19. Destuynder Ph, Djaoua M. Sur une interprétation mathématique de l'intégrale de Rice en théorie de la rupture fragile. *Mathematical Methods in the Applied Sciences* 1981; **3**:70–87.

20. Ciarlet PG. *The Finite Element Method for Elliptic Problems*. North-Holland: Armsterdam, 1978.

21. Grisvard P. *Singularities in Boundary Value Problems*. Masson: Paris, 1992.

22. Lasry J, Pommier J, Renard Y, Salaün M. Extended finite element methods for thin cracked plates with Kirchhoff-Love theory. *International Journal for Numerical Methods in Engineering* 2010; **84**:1115–1138.

23. Liu XY, Xia QZ, Karihaloo BL. XFEM for direct evaluation of mixed mode SIFs in homogeneous and bi-materials. *International Journal for Numerical Methods in Engineering* 2004; **59**:1103–1118.

24. Adams RA. *Sobolev Spaces*. Academic Press: New York, London, 1975.

25. Zucchini A, Hui CY, Zehnder AT. Crack tip stress fields for thin, cracked plates in bending, shear and twisting: a comparison of plate theory and three-dimensional elasticity theory solutions. *International Journal of Fracture* 2000; **104**:387–407.

26. Ciarlet PG. Basic error estimates for elliptic problems. In *Handbook of Numerical Analysis*, Vol. II. North-Holland: Amsterdam, 1991; 17-351.

27. Nicaise S, Renard Y, Chahine E. Optimal convergence analysis for the extended finite element method. *International Journal for Numerical Methods in Engineering* 2011; **86**:528–548.

28. Pommier J, Renard Y. Getfem++, an open source generic C++ library for finite element methods. Available from: http://home.gna.org/getfem/.

29. Zehnder AT, Hui CY. Stress intensity factors for plate bending and shearing problems. *Journal of Applied Mechanics* 1994; **61**:719–722.

30. Viz MJ, Potyondy DO, Zehnder AT, Rankin CC, Riks E. Computation of membrane and bending stress intensity factors for thin, cracked plates. *International Journal of Fracture* 1995; **72**:21–38.

31. Lasry J. Calcul de plaques fissurées avec la méthode des éléments finis étendue (XFEM). *PhD Thesis*, 2009.